SAND99-0178C

A semiconductor microlaser for intracavity flow cytometry

Paul L. Gourley, O. Akhil, G. C. Copeland, J. L. Dunne, J. K. Hendricks, and A. E. McDonald, Sandia National Laboratories, Albuquerque, NM 87185

S. K. Skirboll and L. Nihlen, University of New Mexico School of Medicine, Albuquerque, NM 87131

ABSTRACT

Semiconductor microlasers are attractive components for micro-analysis systems because of their ability to emit coherent, intense light from a small aperture. By using a surface-emitting semiconductor geometry, we were able to incorporate fluid flow inside a laser microcavity for the first time. This confers significant advantages for high throughput screening of cells, particulates and fluid analytes in a sensitive microdevice. In this paper we discuss the intracavity microfluidics and present preliminary results with flowing blood and brain cells.

keywords: microfabrication, semiconductors, microlasers, flow cytometry, intracavity spectroscopy, vertical cavity surface-emitting lasers, blood analysis

1. INTRODUCTION

Microfabricated devices for biomedical applications are receiving considerable interest.[1] They encompass many areas of application and basic studies, including assaying and microfluidic devices for cellular and molecular analysis. Microfluidic structures with micron-sized dimensions have been successfully made with glass, silicon, and polymer materials.[2-6] We have used compound semiconductors with glasses to form microfluidic structures.[7-11] These semiconductors have the advantage of acting as light sources which can probe analytes or cells flowing in the channels. Also, these materials can be configured into microcavity lasers with intracavity flow. The cavities are dichroic, to allow visual imaging of the flow while simultaneously recording lasing spectra at longer wavelengths.

As fluids and cells flow through these channels, their optical properties will alter the emitted lasing spectrum. This lasing technique has been found to detect subtle changes in cellular compositions that are orders of magnitude smaller than can be observed by standard optical microscopy.[12] In addition, this device does not alter the cells, allowing for direct observation of cellular events in the physiologic condition. [9 Previous experiments with static fluids in the microcavity have shown the potential to probe the human immune system (caliper cell and nucleus dimensions of lymphocytes), characterize genetic disorders, and distinguish cancerous and normal cells from tumors.[8] Conceivable future applications of the laser include tumor recognition, blood testing, real time cell characterization, and drug testing.

The application of such a portable biological sensing device could be far-reaching. One practical application of this biocavity laser may be in flow cytometry. Conventional flow cytometers tend to be large, expensive instruments. Thus, a portable device that requires only microleters of blood for analysis would decrease costs and ease operation. It could find widespread use in point of care settings, physicians offices, emergency rooms, or remote battlefield settings.

In order to analyze biological events of cells occurring within these fluids, it is necessary to understand flow behavior within microchannels. In this paper we report the microfabrication of such structures and experimentally examine the intracavity microfluidics. We have measured the average fluid velocity within the microchannels as a function of width, depth, and length for various fluids and as a function of the condition of the channel surface. We also present initial results of flowing blood cells, normal human astrocytes and glioblastoma cells.

2. MICROFABRICATION

The microdevice has been described previously with static fluids.[7-11] This paper describes the first flowing liquids through the micro device. The cavity was formed by optically contacting a semiconductor wafer with a glass chip patterned by microlithography. The semiconductor comprises an optical gain region on a reflecting multilayer. The glass chip was machined with inlet/outlet holes before lithographic patterning. The pattern comprises inlet/outlet regions , deep reservoirs, and shallow flow channels as illustrated in Fig. 1.

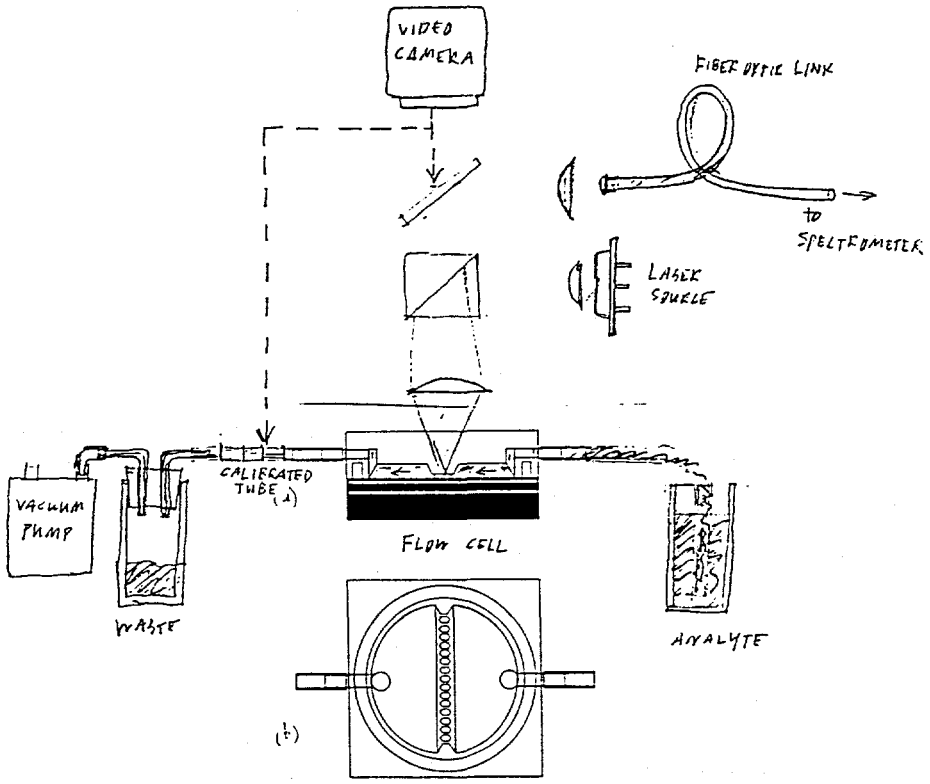

1. Schematic diagram of the experimental arrangement and microfabricated flow cell, showing top (b) and cross sectional (a) views.

Glass chips were microfabricated in the following sequence. First, they were cleaned in dilute HF, rinsed in DI water, dried, cleaned in acetone and isopropyl, rinsed in DI and dried, spun at 5000 rpm for 30 s with a drop of isopropyl, set on hotplate for 5 min at 90 C. placed on spinner, HMDS applied, photoresist AZ5214 supon at 4000 rpm fo r30 s to a final thickness of 1.6 microns. baked at 90 C fo r 2 min. exposed with uv light and developed in 4:1 soln of AZ400K developer and DI water. Resist baked again for 5 min at 90C. Etched in a 2:1 soln of HF to DI for seconds to minutes, depending on final depth required. Rinsed in DI and dried, 4 min acetone bath to strip resist, followed by 20 s in isopropyl alcohol. Rinsed, dried and profiled to determine the final etch depth. Using only photoresist as mask, etch depths in the range 10 to 20 microns could be achieved before undercutting became severe.

After fabrication, the dimensions of the channels were determined by stylus profiling and laser scanning confocal microscopy. The dimensions of the microchannels ranged in width (10-50 um), depth (1-25 um) , and length (90-500 um) to give varying geometric configurations. The number of channels within the flow cell was consistent, ranging from 12-16. This range produces a difference in three orders of magnitude in the hydraulic conductance (R2/L), a geometrical factor (defined below) that determines the flow rates in the channels. These different dimensions allow for difference cell sizes and cell velocities.

After the flow channels were characterized, the patterned surface was coated with a multilayer dielectric reflector and subsequently treated with a polymer or other molecular coating to functionalize the surface for flow. The glass and semiconductor materials were held together in optical contact. The contacting

DISCLAIMER

surfaces were observed under an optical microscope to observe interference fringes. The fringes were used to ensure close contact and to characterize the uniformity of the contacting surfaces. The fringes indicated that the contacted surfaces were very parallel and no less than a few tens of nanometers apart.

3. MICROFLUIDICS IN LASER FLOWCHIP

The average velocity, v, at any flow section A is defined by the following equation:

$$v = Q/A = 1/A \iint \mathbf{v} \cdot d\mathbf{A} \quad (1)$$

Solving this equation for a viscous fluid in laminar flow yields the Hagen-Poiseuille equation for the average flow velocity in a channel,[13,14]

$$v = \Delta p\, r_h^2 / 2L\eta \quad (2)$$

where Δp is the externally applied pressure differential, r_h is the hydraulic radius A/P (channel cross sectional area A divided by perimeter P), L is the channel length, and η is the viscosity of the fluid. For a circular cross section $r_h = D/4$ where D is the inner diameter. For a rectangular cross section $r_h = wd/2(w+d)$ where w and d are the width and depth, respectively. This reduces to $r_h = w/4$ for a square. For water solution eqn 2 can be evaluated as $v=1500\text{mm/s}\ (\Delta p/14.7\text{psi})(A/L6\times10^{-4}\ \text{mm})$. The volume flow rate is constant at every point in the incompressible fluid circuit and given by $Q = vA$. Alternately, the flow rate can be written as $Q = \Delta pG$ where G is a hydraulic conductance. The conductance is $G = (1/2L\eta)(\pi/4)(D^4/16)$ for a circular cross section, $G = (1/2L\eta)(\pi/4)(D^4/16)$ for a square, and $G = (1/2L\eta)d^3w$ for a thin rectangle.

The geometry of the glass flow chip is illustrated in Fig. 1. It comprises machined inlet and outlet holes, provision for contact sealing, deep etch inlet and outlet reservoirs, and a parallel array of flow channels with tapered inlet/outlet. The machined holes are fitted with stainless steel tubing that couple to biocompatible tygon tubing. In the flow experiments, the tip of the inlet (outlet) tubing is placed in a microvial containing the flow (waste) liquid. Thus, the flow system comprises three regions, the tubing, reservoirs, and flow channels. The dimensions of each region is detailed in table I for chips designed for blood analysis.

Table I. Microfluidic parameters of the three cavity regions

region	D/d/w (cm)	A (cm^2)	L (cm)	G (cm^4s/g)	v(cm/s) @7psi $=5\times10^5$ g/cms^2	po ($dyne/cm^2$)
feeder tube	2.5×10^{-2}/na/na	5×10^{-4}	15	6.3×10^{-8}	65	1.1×10^{4}
reservoir *	na/3.5×10^{-3}/0.7	2.5×10^{-3}	0.27	5.6×10^{-6}		4.1×10^{4}
16 channels		8×10^{-6}		7.3×10^{-10}		
1 channel	na/3×10^{-4}/1.7×10^{-3}	5.1×10^{-7}	5×10^{-2}	4.6×10^{-11}	30	5.6×10^{5}

*The reservoir geometry is a half disk with cross sectional area varying with distance x from the inlet to the barrier as $a=t(2xr-x^2)^{1/2}$ r is the radius and t is the depth. This can be approximated by a thin rectangular cross section of width 2r and length $(\pi/4)r$.

The flow rate can be estimated by solving $Q = \Delta pG$ where $1/G = 1/(2/G_1 + 2/G_2 + 1/NG_3)$ and the indices refer to the three regions of the flow circuit and N is the total number of channels. By continuity of an incompressible fluid, vA=constant through the fluid circuit. Thus, the velocity in a give region is $v = \Delta pG/A$. Using the parameters in Table I, the flow rate is limited by the small channel cross section to $Q = 3.7\times10^{-4}$ cm^3/s or 0.37 μL/s. This translates to a velocity of 0.7 cm/s in the feeder tube, 0.15 cm/s in the reservoirs, and 30 cm/s in the channels.

Initially, the flow surfaces are dry and the fluid must pass through the feeder, reservoir, and to the channels, and to the opposite side reservoir, and feeder out. The fluid has forward momentum as it is driven into

these chambers, but encounters a resistive force due to surface tension. The pressure to overcome this force is greater if the cavity is wet with a static fluid than if the fluid has momentum. The pressure to overcome a the static fluid resistance is

$$p_0 = \tau\, C/A \cos\alpha \qquad (3)$$

where τ is the static surface tension, α is the wetting angle, C is the circumference of the cavity and A is the cross sectional area. The values of p_0 with α=90° for the three different cavity regions are summarized in Table I. For typical experiments, p_0 is 7 psi for a 3x20 μm^2 channel. In the channel, p_0 is substantially higher than the values for the other regions. In fact, the value approaches the upper limit of the vacuum pump providing the pressure differential. Small channels can create a problem when a bubble passes through the cavity. In this condition, the fluid can become "stuck" in the channel, prevent any further flow. This "fluid lock" condition requires the cavity to be disassembled, dried, and reassembled to allow flow operation.

3.1 Flow Experiments

An experimental setup to determine the flow rates in the microchip is illustrated in Fig. 1. The inlet and outlet ports of the flow cell were attached to biocompatible Tygon microbore tubing (commerically used as catheters for intravenous and arterial infusion). The outlet line is connected to a miniature vacuum pump through a fluid/vacuum isolation vial where the exiting fluid is allowed to collect. The average measured vacuum pump pressure was 9.3 in. Hg from atmospheric pressure. The inlet line is placed directly into a micro vial contain the test fluid. A video camera was setup to image the moving meniscus of the fluid in the outlet velocity, which was later determined using a TV/VCR playback system.

Before testing the flowchip, the velocity of fluid in isolated tubing was studied to assess the accuracy of Eqn 2. Tubing, which ranged in diameter from .010" to .050" was attached to the pump. The outlet tubing was marked every 0.5 cm lengthwise. Fluids of different viscosity, including water, methanol, and ethylene glycol were flowed through the tubing, and velocity was measured as a function of time and diameter.

The measurement of fluid velocity in the channels is more complicated. Although the fluid velocity in the channels was not directly measured, it was calculated knowing the outlet velocity, outlet cross-sectional area, and channel cross-sectional area. The continuity equation for the volume rate of steady flow of incompressible fluids indicates that there is only one independent variable, v, measured along the centerline of the flow channel. Because of the small size of the channels, most of the resistance to fluid flow occurs here, and thus, we can ignore the contribution to the velocity due to the tubing and reservoirs.

3.2 Results and discussion

The thin solid line in fig. 3 is the theoretical velocity predicted by Eqn 2. This equation applies only to fully developed laminar flow that occurs at a sufficient distance from the entrance, beyond the entrance transition length. The experimental conditions reported here satisfy this requirement. However, this equation does not take into account surface roughness or other surface effects. These factors were ignored due to the low Reynolds number R for these systems (typically R=10-20), describing the ratio of the time rate of momentum change to viscous force, indicating that turbulence is damped out by viscous action.

Results for three different fluids (water, methanol, and ethylene glycol) in tygon tubing are shown as open points in Fig. 3. The velocity is plotted against a hydraulic conductance factor given by the hydraulic radius squared divided by the tube length. So that the flows can be compared more accurately to theory, the data points are corrected for differences in viscosity. The measured velocity is multiplied by the ratio of the viscosity relative to that of water. The data points fall close to the theoretical line, indicating that the functional dependence and magnitude of the flow velocity is well behaved in tygon microtubing.

The results for water flowing in microchannels are shown by the solid circles. At high values of the hydraulic conductance above 10^{-6} cm, these data follow the funtional form of the Hagen-Poiseuille

equation shown by the best fit curve (thick solid line in Fig. 3), but are lower in magnitude by a factor of about 8. Below conductance values of 10^{-6} cm, the measured velocity is limited to values near 4 cm/s. The constant values of velocity measured at very low conductance are probably due to leakage of fluid over the channel barriers. It could also be related to the quality of the fluid sealing around the reservoirs.

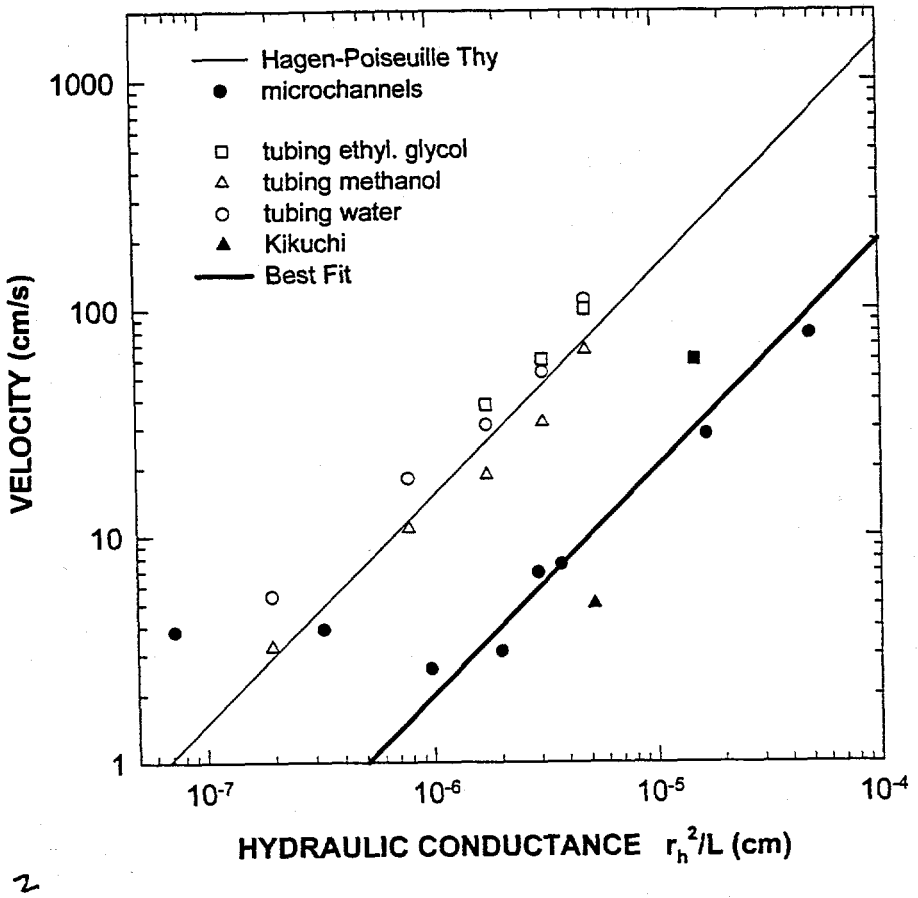

Fig. 2. Velocity vs. Hydraulic Parameter (r^2/L), where r = hydraulic radius and L = tube/channel length. Results shown for tubing (water, methanol, and ethylene glycol), and microchannels.

These differences between experiment and theory at high conductance may be reconciled in part by the interpretation of the hydraulic radius r_h in the Hagen-Poiseuille eqn. The data points in Fig. 3 are plotted with r_h for a rectangular duct, using the width and depth determined by stylus profiling. However, these profiles are far from rectangular due to the chemical undercutting of the resist mask. Trapezoidal shaped ducts[14] offer more flow resistance and the computed r_h would decrease by some 30%, but cannot account for the factor of 8. The observed profile sidewalls have exponential tails that greatly increase the perimeter but not the area. By graphically estimating r_h using the measured profile, we find a nearly two-fold decrease in r_h compared with the rectangular result. This smaller value would produce a 4x shift of the data points to lower conductance, within a factor of 2 of the theory.

Despite this reconciliation, there remains a factor of about 2 difference between experiment and the simple theory. This residual difference may relate to microstructure in the fabricated channel surfaces. For the channels corresponding to the solid data points, no intentional modification of the surfaces was made after microfabrication. A selected channel (solid square) was silanized to make the surface hydrophobic. The measured flow velocity in this channel increased about 2x over the unmodified result.

For comparison, a data point (open crossed point) froom the data of Kikuchi et al.[6] Is shown in Fig. 2. Kikuchi et al. used etched silicon channels (d=4.5 μm, w=7μand L=30μm) in contact with flat glass and fully oxidized surfaces to make them hydrophilic. They performed flow experiments with whole blood, but

used several hundreds of channels in parallel to increase the total volume flow. The channel velocity extracted from their volume flow measurements is only slightly lower than the values obtained in our experiments. This is in spite of the fact that our channels are in glass contacted to a flat gallium arsenide wafer

5. PRELIMARY EXPERIMENTS WITH FLOWING CELLS

5.1 Microflow Laser Spectroscopy for Quantifying Anemia

Estimates suggest that 20% of the world's population suffers from various anemias arising from dietary or genetic deficiencies. Although the disease has many causes, the net effect is a decrease in the concentration of hemoglobin in the red blood cells. Standard methods for measuring anemia involve lysing relatively large volumes (10 ml) of whole blood, oxidizing with potassium ferricyanide and potassium cyanide, and performing spectroscopic absorption at 540 nm (position of the oxidized hemoglobin absorption peak).[15,16] This method determines the average hemoglobin concentration in whole blood, but cannot distinguish cellular or plasma hemoglobin or determine the distribution among the cells. We present a new analysis of single cell hemoglobin using a microcavity laser. The method determines the concentration of hemoglobin and its variation among red blood cells using only 1 uL of whole blood diluted in saline.

5.2 Flow of red blood cells

Glass flow channels were specially fabricated to accommodate flowing red blood cells. These channels were nominally 10 um wide, 500 um long and 3 um deep. Approximately 10 μL of whole blood was diluted in 2 mL of isotonic media. This yields a concentration of about $2x10^4$ red blood cells per μL. The cells flowed well through the channels and were recorded with a high speed, shuttered (exposure time of 100 us) video camera. An image from the video camera is shown in Fig. 3a.

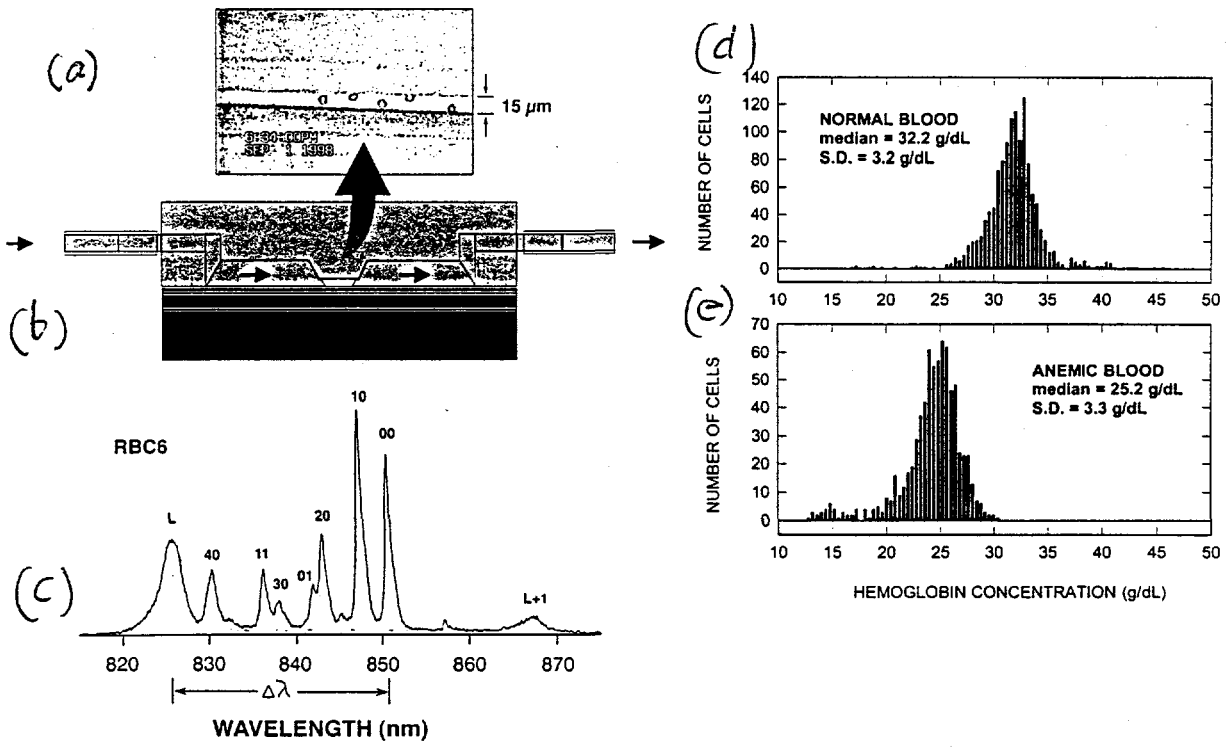

Fig. 3. Results of flowing blood cells through the microcavity. Lasing spectra obtained with a static red blood cell to illustrate the hemoglobin-induced wavelength shift of the fundamental mode. Histograms of individual red blood cell concentration for normal and anemic blood.

The video sequences show that the blood cells are highly deformable and easily pass through the channels without sticking. Cells are initially trapped on barrier region near the channel and launched into the channel at high speed. The cells proceed through the channel one at a time, occasionally bouncing from the channel sidewalls. They remain flat without any rolling motion observed. Since the blood is very dilute, a few platelets and white blood cells are also observed.

The video sequence also allows the cell velocity to be determined directly by measuring the traveled distance during sequential video frames. The cell velocities determined in this manner agree well with the channel fluid velocities determined indirectly by volume flow rates (shown in Fig. 2).

5.3 Intracellular Blood Hemoglobin Measurement

Up to this point, the microflow channels have been passively used for confining cells to flow under an applied pressure. When an external pump laser activates the laser cavity, the cells will trigger the onset of lasing. The emitted lasing spectra can be recorded dynamically with an array detector and analyzed in real time. The following paragraphs describe results of operating the microcavity laser in this condition.

Fig. 3c shows stimulated emission spectra recorded with (solid line) and without (dashed line) the cell present, respectively, in a static fluid microcavity. A dominant peak occurs near 827 nm corresponding to the longitudinal mode of the wet cavity containing only the blood plasma. With the cell present, a series of spectral peaks occurs on the long wavelength side of the longitudinal mode. These peaks correspond to transverse optical modes confined by the red blood cell.[12,17] The rightmost peak in this series is the fundamental transverse mode. Its wavelength shift from the wet cavity mode is directly related to the hemoglobin concentration in the cell. By knowing the effective cavity length and using literature values of the refractive index[18] of hemoglobin solution, the hemoglobin concentration can be determined from the spectra.

The cells were flowed through an active lasing region in a channel and the spectral shift like that in Fig. 3c was determined dynamically. Fig. 4d and e show histograms of such hemoglobin measurements in red cells from normal and anemic blood. The normal red cell histogram shows a mean hemoglobin concentration of about 33 g/dL. In contrast, the anemic red cell histogram shows a much lower mean concentration of 24 g/dL.

5.2 Flow of human brain cells

Newer techniques to further describe and distinguish cells of a neuroepithelial tumor are vital to potentially improving on the current grading schemes for predicting the prognosis of a patient. Real-time analysis of cells in brain tumors not only allows for more timely conclusions on the final diagnosis, but has the potential to assist the neurosurgeon in the operating room. For example, the accuracy of brain biopsies could be verified in the operating room without waiting for the pathologist to process the tissue for a preliminary and sometimes inaccurate diagnosis. Even more important may be capacity for real-time analyses to aid in the actual tumor resection. An ideal surgical tool would utilize an extremely sensitive and efficient method to inform the neurosurgeon immediately that the resection cavity still contains more tumor cells despite the gross appearance of total resection.

To this end we have performed preliminary experiments with normal human astrocytes (NHA) and glioblastoma (GBM) cells. The two cell types are similar in appearance under the microscope, but show distinct spectra in the biocavity laser.[19] These data suggest that the biocavity laser can sensitively probe subtle differences in unstained living cells and additional research and development of this technique could lead to a viable realtime analysis of brain tumor cells.

Specially designed channels were fabricated and the two types of cells, after harvesting from plated cultures were flowed through the channels. The channel dimension was increased over those for blood cells to accommodate these larger cells. Initial experiments in channels with no surface modification showed that both cells tended to stick on the semiconductor surface. A micrograph of the channel region after

flowing GMBs for several minutes is shown in Fig. 6a. The photo reveals multiple cells stuck on the downstream side of the channels. After long times (tens of minutes) the accumulated cells tended to clog the device and severely restrict further flow of cells.

To preclude this effect, we functionalized the microcavity surfaces. The semiconductor was coated with a thin layer of SiO_2 using an ion beam deposition technique. This surface alone was sufficient to enhance the flow time by a factor of 2. Beyond this, the surfaces were further functionalized with polyethylene glycol (PEG) or by silanizing. Both procedures further enhanced the flow time by additional factors of 2 or more. The results of flowing GBM cells on silanized surfaces after several minutes are shown in the micrograph of Fig. 6b. These surface exhibit minimal numbers of sticking cells. Not only did the modified surfaces minimize cell sticking, but also the measure fluid velocity in the channels increased two-fold over that in untreated surfaces (solid square point in Fig. 3). Further studies of surface treatment are warranted to investigate the durability of these molecular layers.

(a) (b)

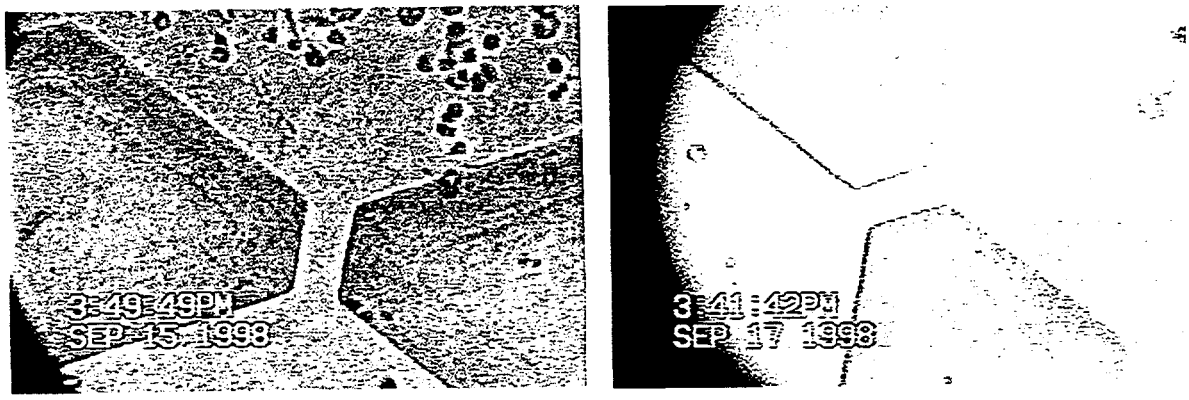

Fig. 4. Optical micrographs of a flow channel after flowing human glioblastoma cells for several minutes. The upper photo is taken with a flow chamber with untreated surfaces. The lower photo is taken with a flow chamber with silanized surfaces.

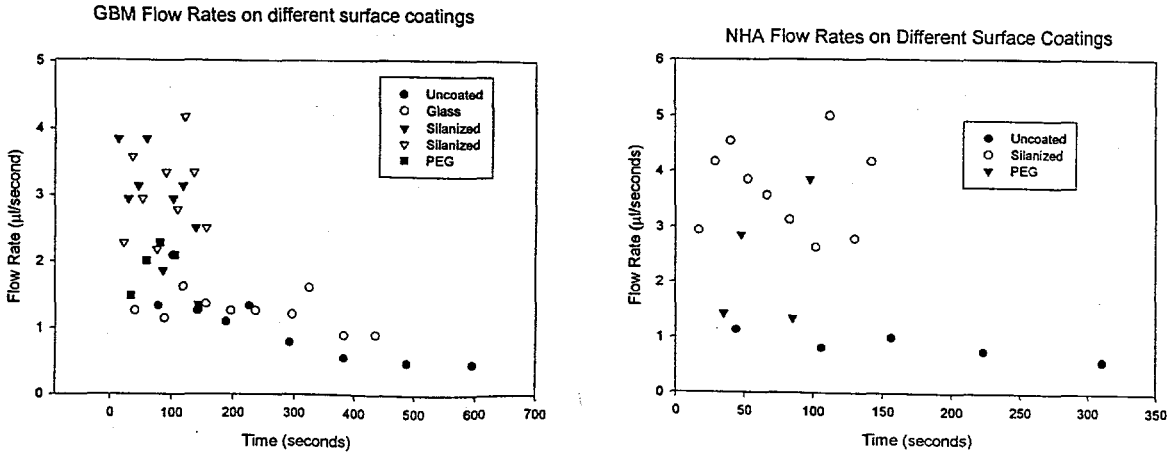

Fig. 6. Fluid flow rates for untreated, PEG, and silane treated surfaces as a function of time.

5

5. DISCUSSION AND SUMMARY

Understanding the microfluidics of the biocavity laser will have a profound effect in the field of physiological fluid analysis. However, these effects are not yet fully understood. Methods for reliably transporting fluids on to and off the semiconductor wafer must be developed in a manner that produces reproducible and accurate results. In this study, we investigated the dependence of channel geometries on fluid velocity and flow. We were able to successfully flow fluid although experimental results varied from the developed Hagen-Poiseuille theory. However, the results behaved of the form of the Hagen-Poiseuille equation, but the absolute value of flow differed considerably. Our results followed the same dependence on geometry, viscosity, and pressure as expected, but deviated consistently by an order of magnitude, suggesting the existence of a common factor.

The effects of flowrate due to factors such as surface roughness and friction were ignored. However, it appears that another surface condition, hydrophilicity, must be studied further. In previous studies, where surfaces were oxidized and thus made hydrophilic, fluid velocity followed theory very closely. Thus, In addition to the disagreement between theoretical and experimental flow, other problems with the flow cell must also be addressed. For example, biocompatibility of the glass and semiconductor wafer is a significant concern. Surfaces must be constructed in such a manner that they do not interact adversely with cells and other biological components. Thus, surfaces must be both hydrophilic and biocompatible in order to characterize accurately the introduced physiological fluids.

Furthermore, if either the semiconductor wafer or glass substrate is not optically flat, poor contact exists. Leaky or nonexistent flow was usually the result. Quality control of both the wafer and glass must be implemented to eliminate this concern. Leaks may also arise from poorly connected tubing, allowing air into the lines. On the other hand, clogging of the tubing and/or channels may result from cells, bacteria, understanding the hydrophilic effects of the current surfaces is imperative to the understanding of the fluidics and consequently to the subsequent applications of the biocavity laser. dust, or other particles being introduced into the flow cell. As was evidenced by the flow of certain cells through the channels, fouling and sedimentation may result, notably in the less deep channels.

Sandia is a multiprogram laboratory operated by Sandia Corporation, a Lockheed Martin Company, for the United States Department of Energy under contract DE-AC04-94AL85000.

REFERENCES

1. See for example. Journal of Biomedical Microdevices, vol 1, 1998.

2. R. H. Carlson, C. V. Gabel, S. S. Chan, R. H. Austin. "White blood cell penetration and fractionation in a microlithographic array," Microfabrication Technology for Biomedical Applications, October 24-25, 1996, San Jose, CA, Conference Notes, Cambridge Healthtech Institute, Upper Newton Falls, MA.

3. D. J. Harrison, K. Fluri, K. Seiler, Z. Fan, C. S. Effenhauser, and A. Manz, Science 261, 895 (1993).

4. J. M. Ramsey, S. C. Jacobson, and M. R. Knapp, "Microfabricated Chemical Measurement Systems," Nature Medicine 1 1093 (1995).

5. R. C. Anderson, G. J. Bogdan, R. J. Lipshutz. "Miniaturized genetic-analysis system," Solid-State Sensor and Actuator Workshop. Hilton Head, South Carolina, pp258-261, June 1996.

6 H. E. Kikuchi, Y. Magariyama, and Y. Kikuchi, Progress in Biomedical Optics, Proc. Micro- and Nanofabricated Structures and Devices for Biomedical and Environmental Applications, SPIE conf. 3258, Jan 26-27, 1998 San Jose, CA, p. 188.

7. P. L. Gourley, *Scientific American*, **278**, 56, 1998.

7. P. L. Gourley et al., "A Radically New Approach to Cell Structure Analysis," Biophotonics International 2, 48-56 (1995).

8. P. L. Gourley et al., Surface-emitting Semiconductor Laser Spectroscopy for Characterizing Normal and Sickled Red Blood Cells, Advances in Laser and Light Spectroscopy to Diagnose Cancer and Other Diseases II: Optical Biopsy, Proc. Biomedical Optics Society, SPIE vol. 2387, 148-161 (1995).

9. P. L. Gourley et al., Vertical Cavity Surface-emitting Laser Scanning Cytometer for High Speed Analysis of Cells, Advances in Laser and Light Spectroscopy to Diagnose Cancer and Other Diseases III: Optical Biopsy, Proc. Biomedical Optics Society, SPIE vol. 2679, 132-141 (1996).

10. P. L. Gourley, "Semiconductor microlasers: A new approach to cell-structure analysis," Nature Medicine, 2, pp 942-944, August 1996.

11. P. L. Gourley, Optics and Photonics News, April 1997, pp. 31-36.
Engineering, **42,** 751 (1995).

12. P. L. Gourley, T. French, A. E. McDonald, E. Shields, and M. F. Gourley, Progress in Biomedical Optics, Proc. Micro- and Nanofabricated Structures and Devices for Biomedical and Environmental Applications, SPIE conf. 3258, Jan 26-27, 1998 San Jose, CA, p. 195.

13. see for example, V. L. Streeter and E. B. Wylie, *Fluid Mechanics*, Mcgraw Hill, New York, 1979.

14. R. K. Shah and A. L. London, *Laminar Flow in Forced* Convection *in Ducts,* Academic Press, New York, 1978.

15. Clinical Hematology and Fundamentals of Hemostasis, 3rd Ed., edited by D. M. Harmening, F. A. Davis Company, Philadelphia, 1997, chap. 3.

16. Ian Russel, Delmar's Clinical Laboratory Manual series: Hematology, Delmar Publishers, New York 1997.

17. B. E. Saleh and M. C. Teich, Fundamentals of Photonics, J. Wiley and Sons, New York, 1991, chap. 8.

18. R. Barer, J. Opt. Soc. Am. 47, 545-52 (1957).

19. Unpublished data, P. L. Gourley and S. K. Skirboll.